Pre-neuronal biomechanical filtering modulates and diversifies whole-hand tactile encoding

Neeli Tummala[1], Gregory Reardon[2], Bharat Dandu[1], Yitian Shao[1,3], Hannes P. Saal[4], Yon Visell[1,2,5,6*]

[1]Department of Electrical and Computer Engineering, University of California, Santa Barbara, Santa Barbara, CA 93106

[2]Department of Media Arts and Technology, University of California, Santa Barbara, Santa Barbara, CA 93106

[3]Department of Electrical and Computer Engineering, Technische Universität Dresden, Germany and Centre for Tactile Internet With Human-in-the-Loop (CeTI), Technische Universität Dresden, Germany

[4]Department of Psychology, University of Sheffield, Sheffield, United Kingdom S10 2TN

[5]Department of Biological Engineering, University of California, Santa Barbara, Santa Barbara, CA 93106

[6]Department of Mechanical Engineering, University of California, Santa Barbara, Santa Barbara, CA 93106

*To whom correspondence should be addressed; E-mail: yonvisell@ucsb.edu.

When the hand touches a surface, the resulting contact elicits skin oscillations that are biomechanically transmitted throughout the hand[1–4], driving responses in an extensive network of exquisitely sensitive Pacinian Corpuscle neurons (PCs)[5–9]. The tuning properties of individual PCs have been well-documented[10–14]. However, such studies employ stimuli applied adjacent to the receptor location, providing little insight into the responses of PCs at any other hand location. When the skin is stimulated by a probe or via manual touch, activity in the majority of PCs is evoked indirectly through

propagating skin oscillations that are further modified by filtering effects of biomechanics[5,15,16]. This biomechanical pathway and its potential implications for tactile information encoding have received little prior attention. Here, we used an integrated approach combining vibrometry imaging and computer simulation to characterize the effects of biomechanical filtering on evoked spiking activity in whole-hand PC populations. We observed complex distance- and frequency-dependent patterns of biomechanical transmission arising from the interplay of tissue mechanics and hand morphology. This source of modulation altered the response properties and spiking activity of PCs, diversifying neural activity in whole-hand PC populations and enhancing information encoding efficiency. These findings suggest that biomechanics furnishes a pre-neuronal mechanism that facilitates efficient tactile processing.

The sense of touch is stimulated when we contact the environment with the skin. Tactile perceptual information is often regarded as originating with the responses of tactile sensory neurons terminating near the contact area. In humans and other animals, touch sensing also arises when the environment is felt indirectly through a probe, such as a tool, rodent whisker, or fingernail. Such probes are not innervated by sensory neurons. Instead, perceptual information is mediated by "internal contacts" that biomechanically couple the probe to sensate tissues innervated by tactile sensory neurons[17]. The same biomechanical couplings that mediate indirect touch are also engaged during direct touch. These couplings facilitate the transmission of evoked skin oscillations to tissues throughout the limb, driving responses in widely distributed mechanoreceptors[1–4].

Indeed, recent findings show that haptic tasks, such as texture exploration[18], dexterous manipulation[19], and tool use[20], generate prominent skin oscillations that are transmitted across the hand. These oscillations convey information about the contact events that initiate them[16,21], which is reflected in responses of Pacinian corpuscle neurons (PCs) throughout the hand[5,7–9]. Thus, during manual touch contact, the intrinsic biomechanics of the hand transforms localized contact forces into spatially distributed skin

oscillations that evoke responses in widespread sensory neurons. The perceptual significance of neural activity in remote receptors is demonstrated by the ability of subjects to perceptually discriminate fine surface textures[3,6] and distinguish vibration frequencies[22] even when the finger is anesthetized by exploiting information encoded in skin oscillations transmitted to remote hand locations. These surprising abilities are consistent with observations that PCs readily respond to subtle vibrations of the ground or other substrates evoked via contact at distant locations[23,24]. Indirectly evoked PC responses also mediate the perception of contact events during object manipulation and tool use[19,20,25] and facilitate the detection of substrate vibrations for perception and communication, as observed in several species[26,27].

Previous studies also suggest that the skin oscillations driving PCs at distinct hand locations are further modified by filtering effects of biomechanics, including frequency- and location-dependent attenuation imparted by the heterogeneous soft tissues of the hand[5,15,16,21]. However, the modulatory effects of biomechanical filtering on the response characteristics of PCs throughout the hand are unknown. Extant peripheral neural recordings reveal PC response behavior to be highly stereotyped, with highest sensitivity between 200 to $300\,\mathrm{Hz}$[10–14]. However, these recordings are obtained from sensory neurons adjacent to the contact location at which the skin is stimulated and do not capture the effects of biomechanical filtering on activity evoked in more distant PCs. Biomechanical filtering could influence the encoding of touch information by whole hand populations of PCs, but such effects and their implications for tactile sensing have received little prior attention.

Imaging whole-hand biomechanical transmission

Here, we characterized the transmission of skin oscillations across the glabrous skin of several human hands (n = 7, P1-P7) and the neural spiking responses evoked in whole-hand PC populations. Mechanical impulses ($0.5\,\mathrm{ms}$ pulse width) were applied at four distinct contact locations, and evoked skin oscillations were recorded at 200 to 350 spatially-distributed locations via optical vibrometry (sample rate $20\,\mathrm{kHz}$, grid spacing $8\,\mathrm{mm}$; see Methods, Fig. 1a). These impulse measurements characterized transmission across the

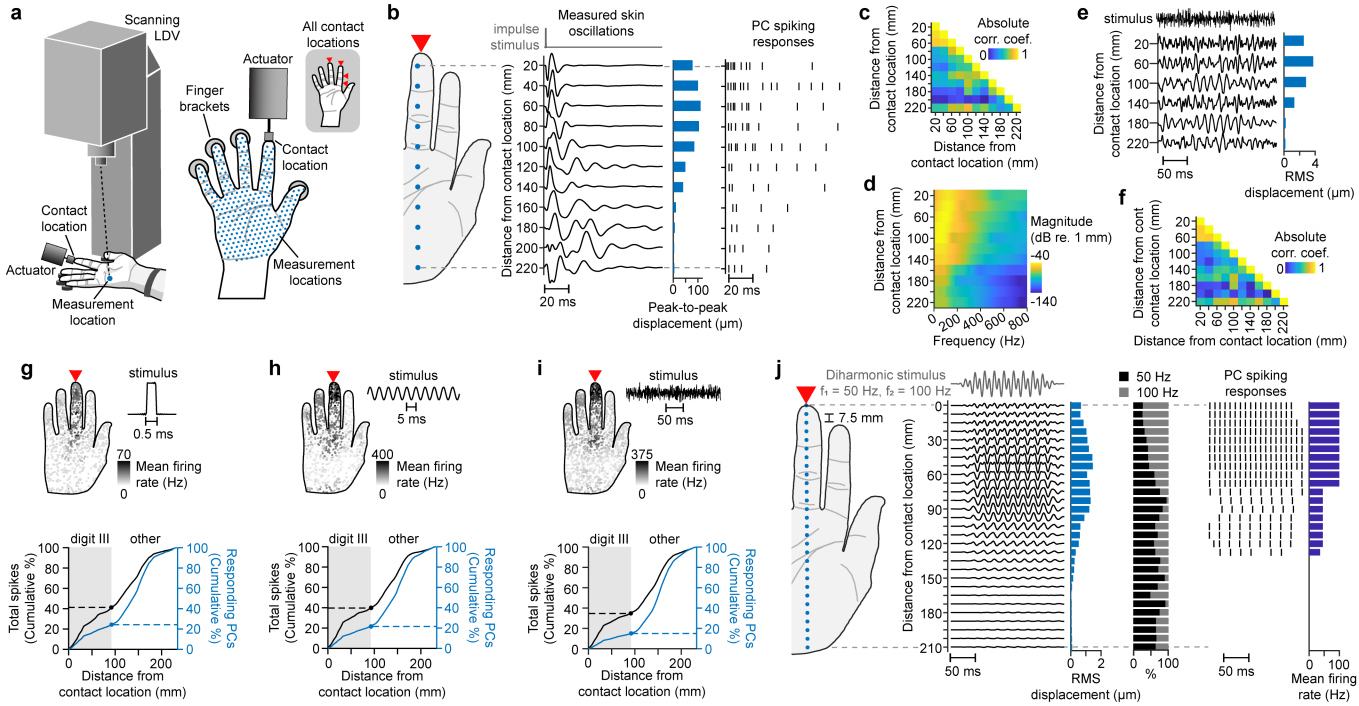

Fig. 1 | Evoked skin oscillations drive location-specific spiking responses in PCs throughout the hand. **a**, Scanning laser Doppler vibrometer (LDV) measurement setup. **b**, Left: vibrometry measurements of skin oscillations at selected locations (blue dots) elicited by an impulse ($0.5\,\mathrm{ms}$ pulse width) applied at the digit III distal phalanx (DP). Right: PC spiking responses evoked by respective skin oscillations, shown for PC neuron model type 4. **c**, Absolute Pearson correlation coefficients between skin oscillations shown in **b**. **d**, Magnitude of frequency spectrum of skin oscillations shown in **b**. **e**, Reconstructed skin oscillations elicited by a bandpass noise stimulus (top trace, 50 - $800\,\mathrm{Hz}$) applied at the digit III DP. **f**, Absolute Pearson correlation coefficients between skin oscillations at different distances from the contact location shown in **e**. **g**, Top: PC mean firing rates elicited by an impulse applied at the digit III DP ($15\,\mu\mathrm{m}$ max. peak-to-peak displacement across hand). Bottom: cumulative percent of spikes (black) and responding PCs (blue) located within increasing distances from the contact location. Shaded region: results within digit III. **h**, As in **g**, for a $200\,\mathrm{Hz}$ sinusoidal stimulus ($15\,\mu\mathrm{m}$ max. peak-to-peak displacement across hand). **i**, As in **g**, for a bandpass noise stimulus (50 - $800\,\mathrm{Hz}$, $5\,\mu\mathrm{m}$ max. RMS displacement across hand). **j**, PC spiking responses (right, PC neuron model type 4) evoked by skin oscillations (middle) at selected locations (left, blue dots) elicited by a diharmonic stimulus ($f_1 = 50\,\mathrm{Hz}$, $f_2 = 100\,\mathrm{Hz}$) applied at the digit III DP. Light blue bars: RMS skin displacements; black and gray bars: percent of frequency magnitude spectrum composed of $50\,\mathrm{Hz}$ (black) or $100\,\mathrm{Hz}$ (gray) components; dark blue bars: PC mean firing rates. All plots show data from Participant 5 (P5).

hand within the frequency range relevant to PCs (20 to $800\,\mathrm{Hz}$). The dispersive nature of biomechanical transmission altered both the temporal structure and frequency content of skin oscillations (Fig. 1b, d). As

a consequence, we observed the pairwise temporal and spectral correlation of skin oscillations at different locations to decrease with increasing pairwise distance (Fig. 1c, d). Due to the linearity of skin biomechanics in the small signal regime[28,29], the impulse measurements accurately encoded the transmission of skin oscillations, which was confirmed in control experiments (see Methods, Extended Data Fig. 1). This allowed us to compute the whole-hand patterns of skin oscillations that would be evoked by arbitrary tactile input waveforms via *in silico* experiments. We reconstructed the evoked skin oscillation patterns by convolving the waveform of interest with the ensemble of recorded impulses (see Methods, Extended Data Fig. 2a). Using this technique, we computed skin oscillations evoked by tactile input signals, including sinusoids, diharmonic signals, and bandpass-filtered noise. This method preserved the modulatory effects of biomechanical filtering, including the phase and amplitude of evoked skin oscillations (Fig. 1e, f).

Biomechanically mediated PC spiking activity

PC spiking responses are driven by deformations of the corpuscle caused by mechanical oscillations of surrounding tissues[14]. Thus, we sought to characterize the location-specific influences of biomechanical filtering on PC spiking responses. Current experimental techniques preclude the *in vivo* measurement of spiking responses of populations of PCs[30]. To overcome this limitation, we obtained whole-hand PC population spiking responses *in silico* by using computationally reconstructed skin oscillations to drive an ensemble of spiking neuron models that were fit to physiological data in prior research[31] (see Methods, Extended Data Fig. 2a). Each PC neuron model was driven by the skin oscillations at its location, and the spatial distribution of PCs across the hand was selected based on findings from a prior anatomical study[32]. We used this methodology to obtain spiking responses from whole-hand populations of PCs as evoked by arbitrary tactile inputs supplied at any of four contact locations on the hand.

Locally supplied stimuli evoked spiking activity in PCs located throughout the hand, consistent with predictions from theory and findings from prior studies[3,5,7]. The majority of responding PCs and spiking

activity originated in hand regions far removed from the contact location. This was observed for all stimulus types, including brief impulses (Fig. 1g), sinusoids (Fig. 1h, Extended Data Fig. 2c), and bandpass noise stimuli (Fig. 1i, Extended Data Fig. 2e). In each case, the effects of biomechanical filtering were reflected in the patterns of evoked spiking activity (Extended Data Fig. 2b, d). The temporal extent and patterns of spiking responses evoked by a brief impulse varied in a location-specific manner, reflecting the complex interplay of PC spiking behavior and modulatory effects of biomechanics, including the dispersive propagation of oscillations in the skin (Fig. 1b). PC responses also exhibited characteristic entrainment behavior (phase-locking to the oscillations of periodic stimuli) modified by location-specific biomechanical filtering. For example, a diharmonic stimulus applied at the fingertip evoked distance-dependent patterns of entrainment: Receptors near the contact location ($< 60\,\mathrm{mm}$) entrained to the higher frequency signal component ($100\,\mathrm{Hz}$), while more distant receptors entrained to the lower frequency component ($50\,\mathrm{Hz}$; Fig. 1j). This distance-dependent entrainment behavior arose due to the greater attenuation of higher frequency skin oscillations with distance (Fig. 1j, black and gray bars), an effect of tissue viscoelasticity.

Spatial dependence of biomechanical filtering

The frequency dependence of biomechanical filtering arises from the viscoelastic characteristics of soft tissues[15], as well as the skeletal structure of the hand. To more systematically characterize these effects, we examined variations in skin oscillations evoked by sinusoidal stimuli of different frequencies, with amplitudes normalized to account for the relative mobility of the skin at different frequencies (see Methods). Skin oscillations elicited by sinusoidal stimuli exhibited complex frequency-dependent amplitude patterns, including non-monotonic decay with distance, particularly at low frequencies (Fig. 2a; results for other participants and contact locations: see Extended Data Fig. 3). We analyzed the frequency-dependent median transmission distance of skin oscillations and observed low-frequency oscillations ($\leq 100\,\mathrm{Hz}$) to be transmitted significantly beyond the stimulated digit. In contrast,

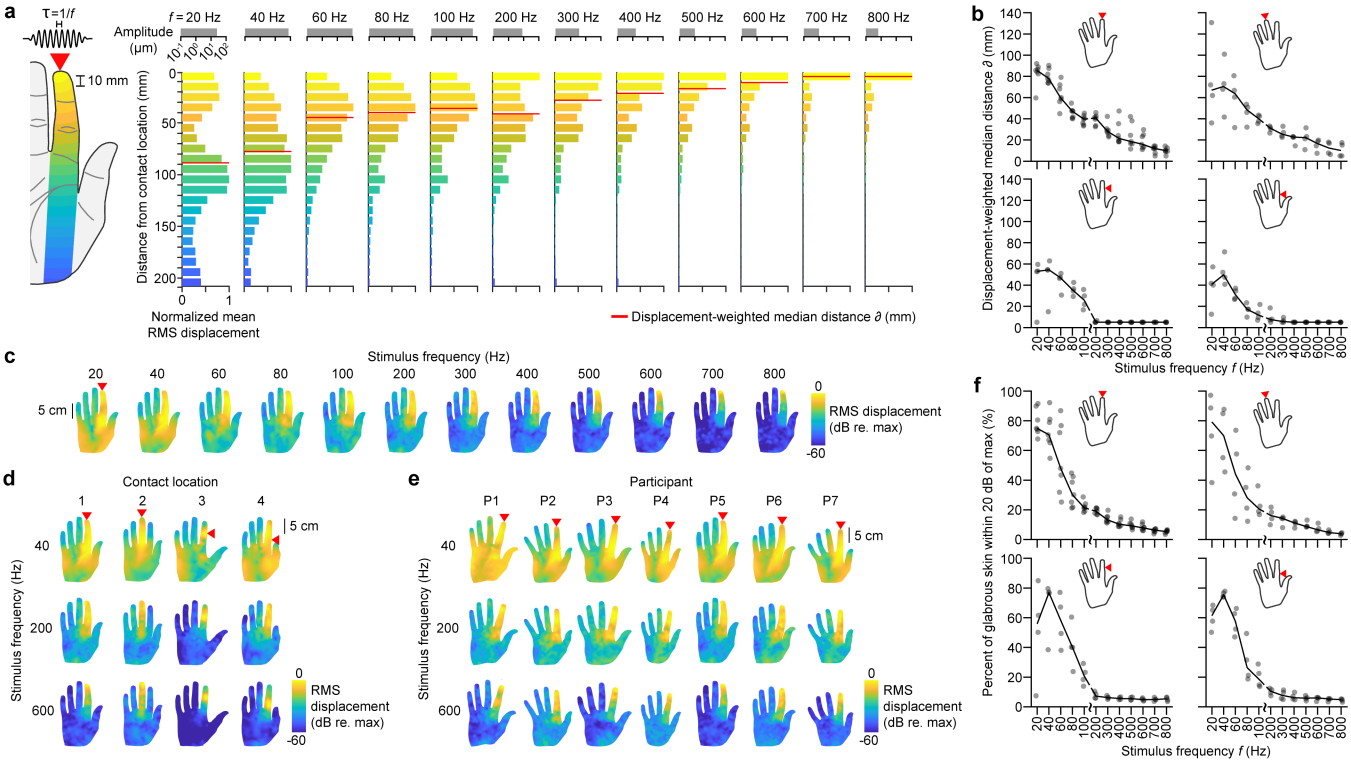

Fig. 2 | Biomechanical filtering in the hand is frequency- and location-dependent. **a**, Normalized distribution of mean root mean square (RMS) skin displacement within 10 mm-wide bands at increasing distances from the contact location elicited by sinusoidal stimuli of various frequencies (20 to 800 Hz). Amplitude scale bars (top, gray) show maximum peak-to-peak displacement across the hand at each frequency. Red lines: median transmission distance; red arrow: contact location. Shown for P5. **b**, Median transmission distance of RMS skin displacement distributions across frequency for all participants and contact locations. Red arrows: contact location; lines: median across participants; dots: data points for each participant. **c**, RMS displacement across the hand elicited by sinusoidal stimuli of various frequencies (20 to 800 Hz). Red arrow: contact location. Shown for P5. **d**, As in **c**, for other contact locations. Shown for P5. **e**, As in **c**, for P1-P7. **f**, Percent of glabrous skin where RMS skin displacement is within 20 dB of the maximum RMS displacement, for all participants and contact locations. Plots can be read as in **b**.

higher-frequency components were predominantly concentrated within the stimulated digit. We obtained similar findings for all hands and stimulus locations (Fig. 2b).

The complex, frequency-dependent patterns of the transmission of skin oscillations across the hand surface were influenced by the heterogeneous morphology and skeletal structure of the hand. At low frequencies (≤ 100 Hz), transmission was notably enhanced near the metacarpophalangeal (MCP) joint of

the stimulated digit and in the lateral and contralateral extensions of the palmar surface (thenar and hypothenar eminences) (Fig. 2c-e; results for all participants and contact locations: see Extended Data Fig. 4). These low-frequency stimuli evoked prominent oscillations (within $20\,\mathrm{dB}$ of maximum) over a substantial fraction of the hand surface (mean $50\,\%$; Fig. 2f). In contrast, higher frequencies evoked skin oscillations over a much smaller proportion of the hand surface (mean $8\,\%$). Findings were consistent across contact locations and participants.

Biomechanical filtering modulates PC tuning

To quantify the effects of biomechanical filtering on PC frequency response characteristics, we next studied whole-hand PC spiking activity evoked by sinusoidal stimuli supplied at each of the four contact locations. We quantified the frequency-dependent sensitivity of PCs by determining entrainment threshold curves that represent the minimum displacement required to evoke entrainment at each frequency (see Methods). PCs located near the contact location exhibited U-shaped entrainment threshold curves with preferred (most sensitive) frequencies between 200 and $300\,\mathrm{Hz}$ (Fig. 3a, Extended Data Fig. 5a). This result is consistent with prior *in vivo* studies of individual PCs performed by applying the stimulus close to the location of the PC[10–14]. In contrast, entrainment threshold curves for PCs away from the contact location varied greatly and exhibited multiple prominent minima due to the location-specific filtering of skin oscillations (Fig. 3a, Extended Data Fig. 5b, c). Moreover, the frequency sensitivity of a given PC varied greatly depending on the contact location (Fig. 3b).

We next examined the diversity in PC frequency response characteristics across whole-hand PC populations by rank ordering entrainment threshold curves by preferred frequency (Fig. 3c, d; results for all participants and contact locations: see Extended Data Fig. 6). Across the population, PCs exhibited diverse preferred frequencies, ranging from 25 to $420\,\mathrm{Hz}$ (Extended Data Fig. 7a-d). The preferred frequencies of PCs located near the contact location were consistent with values obtained in prior studies of individual PCs (200 to $300\,\mathrm{Hz}$), but PCs further away from the contact location had a wider range of

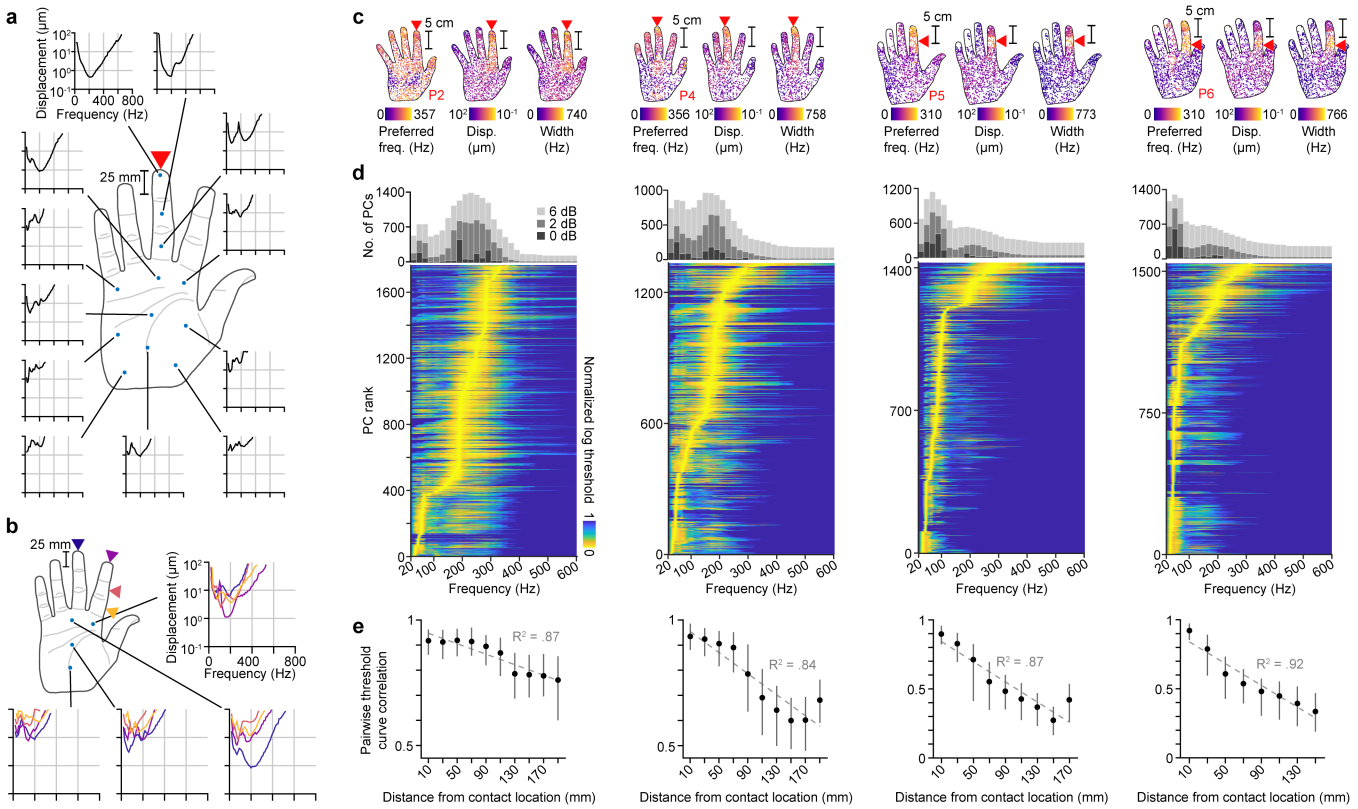

Fig. 3 | Biomechanical filtering diversifies PC response characteristics. a, Entrainment threshold curves of PCs at selected locations (blue dots). Red arrow: Contact location. Shown for PC neuron model type 4 and P1. **b**, Entrainment threshold curves of PCs at selected locations (blue dots) for each of 4 contact locations (colored arrows). Line colors correspond to contact locations. Shown for PC neuron model type 4 and P1. **c**, Preferred frequency (left), minimum curve value (middle), and curve width (right) for each PC in the hand. Red arrow: contact location; red text: participant number. **d**, Lower panel: Entrainment threshold curves for all PCs in the hand rank ordered by preferred frequency. Upper panel: Number of PCs at each frequency with entrainment threshold curve values within $0\,\mathrm{dB}$ (light gray), $+2\,\mathrm{dB}$ (medium gray), and $+6\,\mathrm{dB}$ (dark gray) of the curve minimum. Participants and contact locations as in **c**. **e**, Pairwise Pearson correlation coefficients between all pairs of entrainment threshold curves of PCs located within $10\,\mathrm{mm}$ of the contact location and those of PCs located within $20\,\mathrm{mm}$-wide bands at increasing distances from the contact location. Center distance for each band shown. Dots: median; error bars: IQR; gray dotted lines: linear fit of medians; gray text: R^2 value for linear fit. Participants and contact locations as in **c**.

frequency sensitivities (Extended Data Fig. 7e-h). Strikingly, across all participants and contact locations, a substantial proportion of PCs in a population preferred frequencies below $100\,\mathrm{Hz}$ (mean $47\,\%$). In addition, PCs at greater distances from the contact location were generally less sensitive with elevated

thresholds and exhibited more narrowly tuned curves (Fig. 3c).

However, threshold curves had complex shapes not adequately summarized by preferred frequency or curve width and varied greatly with location. To characterize distance-dependent variations in the entrainment curves, we calculated pairwise correlations between threshold curves of PCs at the contact location and those within regions at progressively greater distances across the hand (see Methods, Fig. 3e; results for all participants and contact locations: see Extended Data Fig. 8). For all participants and contact locations, the median pairwise correlation decreased with increasing distance from the contact location (0.021 to 0.095 per $20\,\mathrm{mm}$; $R^2 = 0.51$ to 0.95). Together, these findings demonstrate that pre-neuronal biomechanical filtering diversified frequency response characteristics in whole-hand PC populations.

Biomechanical filtering diversifies tactile encoding

We next asked whether this diversification enhanced information encoding in PC population spiking responses, particularly for the majority of responding PCs that are distant from the contact location. To answer this question, we characterized the dimensionality and information content of PC population spiking activity as a function of distance from the contact location (see Methods). Informed by prior research[33,34], we analyzed PC activity evoked by a diverse set of stimuli containing sinusoidal, diharmonic, and bandpass noise signals with various frequency and amplitude parameters. First, we characterized the latent dimensionality of PC firing rates in subpopulations of PCs within increasing maximum distances from the contact location. Dimensionality, calculated as the number of principal components needed to capture $99\,\%$ of the variance in the firing rates, was 2 to 5 times higher at distances of more than $100\,\mathrm{mm}$ from the contact location than at distances of less than $20\,\mathrm{mm}$ (Fig. 4a). These findings were consistent across all participants and contact locations. Thus, PCs at increasing distances from the contact location captured progressively more variance, highlighting the facilitative role of biomechanical filtering in PC population encoding.

In addition to firing rates, PCs signal information about touch events in their spike timing[34]. We

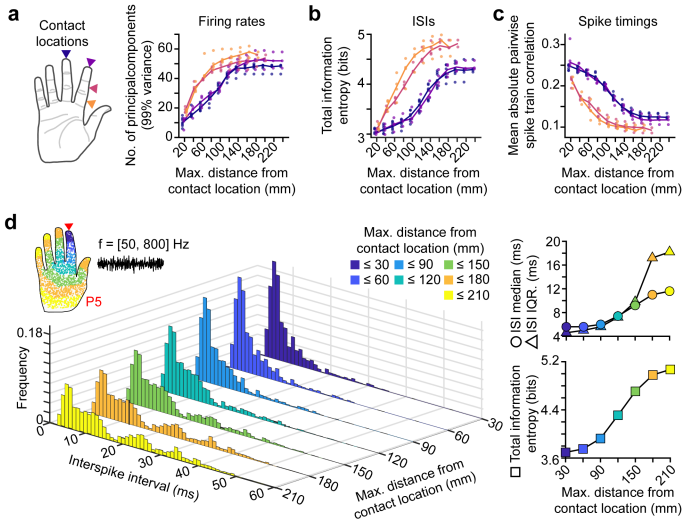

Fig. 4 | Biomechanical filtering diversifies PC spiking activity. **a**, Number of principal components explaining $99\,\%$ of the variance in firing rates for PCs within increasing distance ranges from the contact location, for all participants and contact locations. **a**, **b**, **c**, Colors indicate contact location; colored dots: data points for each participant; lines: median across participants. **b**, Total information entropy of interspike interval (ISI) distributions (bin width: $1\,\mathrm{ms}$), as constructed for PCs within increasing distance ranges from the contact location, for all participants and contact locations. **c**, Mean absolute spike train correlation between all pairs of PCs both located within increasing distances from the contact location, for all participants and contact locations. Spike trains were binned with a bin width of $1\,\mathrm{ms}$. **d**, Left panel: ISI histograms for PCs located within increasing distances from the contact location (hand inset) in response to a bandpass noise stimulus (50 - $800\,\mathrm{Hz}$, $5\,\mu\mathrm{m}$ max. RMS displacement across hand, $175\,\mathrm{ms}$ duration) applied at the digit II DP of P5. Right panels: median (circles), interquartile range (triangles), and total information entropy (squares) of the ISI histograms (left panel).

characterized information encoded in PC spike timing by computing the information entropy of interspike interval (ISI) histograms and correlations between spike trains evoked in subpopulations of PCs within increasing maximum distances from the contact location (see Methods). In all cases, ISIs were larger and more broadly distributed with increasing distance from the contact location (Fig. 4d, Extended Data Fig. 9). As a consequence, information encoded by the ISI histograms, calculated as Shannon entropy, increased monotonically with distance by a factor of more than 1.4 before plateauing at 140 to $180\,\mathrm{mm}$ from the contact location (Fig. 4b). The findings were robust to variations in ISI histogram bin widths (Extended Data Fig. 10a-g). Consistent with these findings, the spiking activity of PCs at increasing

distances was progressively less correlated with the activity of PCs near the contact location, quantified by mean pairwise spike train correlations (Fig. 4c, Extended Data Fig. 10h-n). Together, these findings indicate that biomechanical filtering diversifies PC spiking activity while also preserving a degree of response redundancy among PCs.

Discussion

Our study combined high-resolution vibrometry measurements of whole-hand biomechanical transmission with neural simulations leveraging extensively validated neuron models[31] to elucidate the pre-neuronal role of biomechanical filtering in modulating and diversifying PC population spiking activity. Notably, PC population response characteristics differed markedly from those documented for PCs located adjacent to the contact location. Because the majority of responding PCs are distant from a localized contact stimulus, neural activity in distant PCs represents a dominant proportion of the total population response and can thus be expected to affect downstream tactile processing and, ultimately, perception.

There is ample prior evidence that biomechanically facilitated activity in touch receptors located away from the stimulus contact site influences perceptual processing. Prior findings reveal that the perception of tactile stimuli in both the high frequency ($> 80\,\mathrm{Hz}$) and flutter range ($\sim 20\,\mathrm{Hz}$) can be mediated by PCs that are not located near the site of skin stimulation, as demonstrated in studies employing local anesthesia, ulnar nerve compression, or subjects that experienced digital nerve lesion[22,35,36]. Prior researchers also found that fine surface textures explored with the anesthetized finger can be perceptually discriminated[6], apparently mediated by activity in remote PCs that is indirectly evoked by propagating skin oscillations traveling far from the contact location[3]. Prior findings also highlight the significance of biomechanical transmission for the perception of haptic feedback. The propensity of lower frequency skin oscillations to travel greater distances has been exploited to realize frequency-controlled haptic effects that are perceived to expand or contract in spatial extent from a single localized site of stimulation[15]. Moreover, a recent study revealed that the perception of aeroacoustically supplied tactile motion stimuli is determined by the spatiotemporal

dynamics of biomechanically transmitted skin oscillations[37].

Accounting for the effects of biomechanics on peripheral tactile encoding may also shed light on touch perception in many other settings. For example, the perceived intensity of vibrations depends strongly on stimulation frequency[38,39], but this dependence does not agree with predictions derived based on responses of individual PCs[33]. Moreover, proposed models for the perception of stimuli with complex frequency spectra have invoked the existence of previously unobserved neural subpopulations that vary in frequency selectivity[40], in contrast with the broad and stereotyped frequency tuning properties documented for isolated PCs.

Our findings may also shed light on a number of peculiar aspects of PC innervation of the hand. Despite the stereotyped response properties of isolated PCs and their large receptive fields, which span most of the hand, PCs in the glabrous skin number in the hundreds or more[32,41–43]. Considered in isolation, these characteristics would imply tremendous response redundancy, which would be at odds with encoding efficiency hypotheses[44]. However, our results demonstrate that biomechanical filtering diversifies PC response characteristics, thereby reducing PC population response redundancy and enhancing encoding efficiency. Furthermore, prominent clusters of PCs are observed near the MCP joints in human hands[42,43]. Near those locations, we observed elevated oscillation amplitudes at low frequencies ($<100\,\mathrm{Hz}$), suggesting that PCs may be preferentially located in regions of the hand where biomechanical transmission is facilitated.

The frequency-dependent patterns of biomechanical transmission and filtering we observed are generally consistent with prior characterizations of mechanical propagation in individual fingers[5,15,45], taking into account likely differences in contact conditions. Here, we present whole-hand measurements at significantly greater spatiotemporal resolution than was used in prior studies. This made it possible to resolve the effects of biomechanical transmission and filtering throughout the hand, including pronounced differences between evoked signals disseminated to the fingers and palm, non-monotonic decay of oscillation amplitude with distance, and contact location-dependent variations in filtering across hand

areas. Despite these observed complexities of biomechanical transmission in the hand, several characteristics were conserved across multiple hands and stimulus locations. These include the frequency-dependent variations in transmission amplitude with distance, the elevated transmission distances observed at low frequencies ($\leq 100\,\mathrm{Hz}$), and the enhancement of transmission near the MCP joints. These findings demonstrate how biomechanical filtering generates spatial and spectral structure that the brain could learn and exploit, similar to hypotheses for efficient encoding of whole-hand touch events[16], object slippage[46], and tool use[20].

Overall, the pronounced effect of biomechanics that we observed in the PC system exemplifies how pre-neuronal mechanisms can play a crucial role in sensory processing, which is supported by analogous findings in other sensory systems. For example, the effect of biomechanical filtering on tuning properties across PC populations is somewhat comparable to the frequency-place transform that is biomechanically affected by the mammalian cochlea[47,48], but instead facilitated by the morphology and biomechanics of the hand. Similar conclusions about the impact of biomechanics in sensory processing have also been drawn in studies of the rodent vibrissal system, where the mechanics of the whiskers are instrumental to tactile neural coding[49,50]. Moreover, a recent study based on recordings of PC responses in freely moving mice elucidated prominent effects of biomechanical transmission on PC responses and revealed PC response characteristics to be highly diverse[24], consistent with our findings.

References

1. Moore, T. J. A Survey of the Mechanical Characteristics of Skin and Tissue in Response to Vibratory Stimulation. *IEEE Transactions on Man-Machine Systems* **11,** 79–84 (1970).
2. Pubols, B. H. Effect of Mechanical Stimulus Spread across Glabrous Skin of Raccoon and Squirrel Monkey Hand on Tactile Primary Afferent Fiber Discharge. *Somatosensory Research* **4,** 273–308 (1987).
3. Delhaye, B., Hayward, V., Lefèvre, P. & Thonnard, J.-L. Texture-induced vibrations in the forearm during tactile exploration. *Frontiers in Behavioral Neuroscience* **6** (2012).
4. Shao, Y., Hayward, V. & Visell, Y. Spatial patterns of cutaneous vibration during whole-hand haptic interactions. *Proceedings of the National Academy of Sciences* **113,** 4188–4193 (2016).
5. Manfredi, L. R. *et al.* The Effect of Surface Wave Propagation on Neural Responses to Vibration in Primate Glabrous Skin. *PLOS ONE* **7,** e31203 (2012).
6. Libouton, X., Barbier, O., Berger, Y., Plaghki, L. & Thonnard, J.-L. Tactile roughness discrimination of the finger pad relies primarily on vibration sensitive afferents not necessarily located in the hand. *Behavioural Brain Research* **229,** 273–279 (2012).
7. Andrews, J. W., Adams, M. J. & Montenegro-Johnson, T. D. A universal scaling law of mammalian touch. *Science Advances* **6,** eabb6912 (2020).
8. Corniani, G., Casal, M. A., Panzeri, S. & Saal, H. P. Population coding strategies in human tactile afferents. *PLOS Computational Biology* **18,** e1010763 (2022).
9. Tummala, N., Shao, Y. & Visell, Y. *Spatiotemporal organization of touch information in tactile neuron population responses* in *2023 IEEE World Haptics Conference (WHC)* (2023).
10. Sato, M. Response of Pacinian corpuscles to sinusoidal vibration. *The Journal of Physiology* **159,** 391–409 (1961).
11. Talbot, W. H., Darian-Smith, I., Kornhuber, H. H. & Mountcastle, V. B. The sense of flutter-vibration: comparison of the human capacity with response patterns of mechanoreceptive afferents from the monkey hand. *Journal of Neurophysiology* **31,** 301–334 (1968).
12. Johansson, R. S., Landström, U. & Lundström, R. Responses of mechanoreceptive afferent units in the glabrous skin of the human hand to sinusoidal skin displacements. *Brain Research* **244,** 17–25 (1982).
13. Bolanowski, S. J. & Zwislocki, J. J. Intensity and frequency characteristics of pacinian corpuscles. I. Action potentials. *Journal of Neurophysiology* **51,** 793–811 (1984).
14. Bell, J., Bolanowski, S. & Holmes, M. H. The structure and function of pacinian corpuscles: A review. *Progress in Neurobiology* **42,** 79–128 (1994).
15. Dandu, B., Shao, Y. & Visell, Y. Rendering Spatiotemporal Haptic Effects Via the Physics of Waves in the Skin. *IEEE Transactions on Haptics* **14,** 347–358 (2020).

16. Shao, Y., Hayward, V. & Visell, Y. Compression of dynamic tactile information in the human hand. *Science Advances* **6** (2020).

17. Gibson, J. *The senses considered as perceptual systems* (Houghton Mifflin, Oxford, England, 1966).

18. Bensmaia, S. J. & Hollins, M. The vibrations of texture. *Somatosensory & Motor Research* **20,** 33–43 (2003).

19. Johansson, R. S. & Flanagan, J. R. Coding and use of tactile signals from the fingertips in object manipulation tasks. *Nature Reviews Neuroscience* **10,** 345–359 (2009).

20. Miller, L. E. *et al.* Sensing with tools extends somatosensory processing beyond the body. *Nature* **561,** 239–242 (2018).

21. Manfredi, L. R. *et al.* Natural scenes in tactile texture. *Journal of Neurophysiology* **111,** 1792–1802 (2014).

22. Nagi, S. S. *et al.* Contribution of remote Pacinian corpuscles to flutter-range frequency discrimination in humans (2023).

23. Hunt, C. C. & McIntyre, A. K. Characteristics of responses from receptors from the flexor longus digitorum muscle and the adjoining interosseous region of the cat. *The Journal of Physiology* **153,** 74–87 (1960).

24. Turecek, J. & Ginty, D. D. Coding of self and environment by Pacinian neurons in freely moving animals (2023).

25. Brisben, A. J., Hsiao, S. S. & Johnson, K. O. Detection of Vibration Transmitted Through an Object Grasped in the Hand. *Journal of Neurophysiology* **81,** 1548–1558 (1999).

26. Gregory, J. E., McIntyre, A. K. & Proske, U. Vibration-evoked responses from lamellated corpuscles in the legs of kangaroos. *Experimental Brain Research* **62,** 648–653 (1986).

27. Bouley, D., Alarcon, C., Hildebrandt, T. & O'Connell-Rodwell, C. E. The distribution, density and three-dimensional histomorphology of Pacinian corpuscles in the foot of the Asian elephant (Elephas maximus) and their potential role in seismic communication. *Journal of anatomy* **211** (2007).

28. Fradet, C., Manfredi, L. R., Bensmaia, S. & Hayward, V. *Fingertip skin as a linear medium for wave propagation* in *2017 IEEE World Haptics Conference (WHC)* (2017), 507–510.

29. Tummala, N. *et al. SkinSource: A Data-Driven Toolbox for Predicting Touch-Elicited Vibrations in the Upper Limb* in *2024 IEEE Haptics Symposium* (2024).

30. Deflorio, D., Di Luca, M. & Wing, A. M. Skin and Mechanoreceptor Contribution to Tactile Input for Perception: A Review of Simulation Models. *Frontiers in Human Neuroscience* **16** (2022).

31. Saal, H. P., Delhaye, B. P., Rayhaun, B. C. & Bensmaia, S. J. Simulating tactile signals from the whole hand with millisecond precision. *Proceedings of the National Academy of Sciences* **114,** E5693–E5702 (2017).

32. Johansson, R. S. & Vallbo, A. B. Tactile sensibility in the human hand: relative and absolute densities of four types of mechanoreceptive units in glabrous skin. *The Journal of Physiology* **286,** 283–300 (1979).

33. Muniak, M. A., Ray, S., Hsiao, S. S., Dammann, J. F. & Bensmaia, S. J. The Neural Coding of Stimulus Intensity: Linking the Population Response of Mechanoreceptive Afferents with Psychophysical Behavior. *Journal of Neuroscience* **27,** 11687–11699 (2007).

34. Mackevicius, E. L., Best, M. D., Saal, H. P. & Bensmaia, S. J. Millisecond Precision Spike Timing Shapes Tactile Perception. *The Journal of Neuroscience* **32,** 15309 (2012).

35. Morley, J., Hawken, M. & Burge, P. Vibratory detection thresholds following a digital nerve lesion. *Experimental brain research* **72,** 215–218 (1988).

36. Mahns, D. A., Perkins, N. M., Sahai, V., Robinson, L. & Rowe, M. J. Vibrotactile Frequency Discrimination in Human Hairy Skin. *Journal of Neurophysiology* **95,** 1442–1450 (2006).

37. Reardon, G., Dandu, B., Shao, Y. & Visell, Y. Shear shock waves mediate haptic holography via focused ultrasound. *Science Advances* **9,** eadf2037 (2023).

38. Stevens, S. S. Tactile vibration: Change of exponent with frequency. *Atten. Percept. Psychophys.* **3,** 223–228 (1968).

39. Verrillo, R. T., Fraioli, A. J. & Smith, R. L. Sensation magnitude of vibrotactile stimuli. *Atten. Percept. Psychophys.* **6,** 366–372 (1969).

40. Bensmaia, S., Hollins, M. & Yau, J. Vibrotactile intensity and frequency information in the Pacinian system: A psychophysical model. *Perception & Psychophysics* **67,** 828–841 (2005).

41. Corniani, G. & Saal, H. P. Tactile innervation densities across the whole body. *Journal of Neurophysiology* **124,** 1229–1240 (2020).

42. Stark, B., Carlstedt, T., Hallin, R. G. & Risling, M. Distribution of Human Pacinian Corpuscles in the Hand: A cadaver study. *Journal of Hand Surgery* **23,** 370–372 (1998).

43. Germann, C., Sutter, R. & Nanz, D. Novel observations of Pacinian corpuscle distribution in the hands and feet based on high-resolution 7-T MRI in healthy volunteers. *Skeletal Radiology* **50,** 1249–1255 (2021).

44. Barlow, H. B. in *Sensory Communication* (ed Rosenblith, W. A.) (The MIT Press, 1961).

45. Wiertlewski, M. & Hayward, V. Mechanical behavior of the fingertip in the range of frequencies and displacements relevant to touch. *Journal of Biomechanics* **45,** 1869–1874 (2012).

46. Willemet, L., Huloux, N. & Wiertlewski, M. Efficient tactile encoding of object slippage. *Scientific Reports* **12,** 13192 (2022).

47. V. Békésy, G. Human Skin Perception of Traveling Waves Similar to Those on the Cochlea. *The Journal of the Acoustical Society of America* **27,** 830–841 (1955).

48. Saal, H., Wang, X. & Bensmaia, S. Importance of spike timing in touch: an analogy with hearing? *Current Opinion in Neurobiology* **40,** 142–149 (2016).

49. Bagdasarian, K. *et al.* Pre-neuronal morphological processing of object location by individual whiskers. *Nat. Neurosci.* (2013).

50. Ding, Y. & Vlasov, Y. Pre-neuronal processing of haptic sensory cues via dispersive high-frequency vibrational modes. *Sci. Rep.* **13,** 14370 (2023).

Methods

In vivo optical vibrometry

Mechanical oscillations across the volar hand surface were imaged with a scanning laser Doppler vibrometer (SLDV; model PSV-500, Polytec, Inc., Irvine, CA; sample frequency $20\,\mathrm{kHz}$) fastened to a pneumatically isolated table. During each recording, the hand was fixed to the table in an open, palm-up posture via custom-fit 3D printed supports that were fastened to the table and adhered to the fingernails of all but the stimulated digit (Fig. 1a). Participants ($n = 7$, 5 male) were 20 to 45 years of age (mean 27.4 years) and were recruited from the student and staff population at the authors' institution. They were seated in a reclined chair with the arm relaxed, supported by a foam armrest, and constrained with Velcro straps. All subjects gave their informed, written consent prior to the data collection. The study was performed in accordance with the Declaration of Helsinki and was approved by the Human Subjects Committee of the University of California, Santa Barbara (Protocol Number 9-18-0676).

The SLDV imaged spatially and temporally resolved skin oscillations at sampling locations distributed on a uniform grid covering the entire volar hand surface (grid spacing $8\,\mathrm{mm}$, 200 - 350 locations). The sampling grid exceeded the Nyquist criterion threshold for frequencies in the tactile range (0 to $1000\,\mathrm{Hz}$), which exhibit spatial wavelengths between 20 and $100\,\mathrm{mm}$[16]. Oscillations were imaged in the normal direction to the skin surface. Prior vibrometry measurements have demonstrated that most of the energy in evoked skin oscillations is concentrated in oscillations normal to the skin surface[15] and that stress in the normal direction is highly predictive of PC spiking responses[31].

All data were captured from the right hands of participants. Hand lengths ranged from 18 to $21.6\,\mathrm{cm}$ (mean $19.9\,\mathrm{cm}$) as measured from the tip of digit III to the bottom of the hand at the middle of the wrist. Each hand was positioned $360\,\mathrm{mm}$ below the SLDV aperture, which ensured that the measurements captured at least $95\,\%$ of the signal variance at all measurement locations. Hand shape and 2D spatial coordinates of all measurement locations were captured via the integrated SLDV geometry processor and

camera. Measurements were interpolated to obtain skin oscillations at other locations on the 2D hand surface (see Supplementary Methods).

Measured skin oscillations were evoked by mechanical impulses (rectangular pulse, duration $0.5\,\mathrm{ms}$) applied at each of the four contact locations described below. Measurements were synchronized to the stimulus onset. Each measurement was obtained as the median of 10 captures and bandpass filtered to the vibrotactile frequency range (20 to $1000\,\mathrm{Hz}$). Numerical frequency-domain integration was employed to obtain skin displacement from velocity. Stimuli were delivered via an electrodynamic actuator (Type 4810, Brüel & Kjær) driven with a laboratory amplifier (PA-138, Labworks). The actuator terminated in a plastic probe ($7\times7\,\mathrm{mm}$ contact surface) that was adhesively attached to the skin at the stimulus contact location. The actuator and probe were configured to avoid obstructing the optical path used for the SLDV measurements.

Stimuli were applied at each of four different contact locations registered to the respective hand anatomy: the distal phalanx (DP) of digit II along the axis of the finger (Contact Location 1, n = 7 participants), the DP of digit III along the axis of the finger (Contact Location 2, n = 4), the intermediate phalanx (IP) of digit II perpendicular to the axis of the finger (Contact Location 3, n = 4), and the proximal phalanx (PP) of digit II perpendicular to the axis of the finger (Contact Location 4, n = 4) (Fig. 1a). These measurements took approximately 10 minutes per contact condition per participant. Measurements for Contact Locations 2, 3, and 4 were performed on participants who were a subset of the participants measured for Contact Location 1 (P1, P4, P5, and P6).

Computing skin oscillations evoked by arbitrary stimuli

Theory and experimental findings[28,29] indicate that biomechanical transmission in the hand is linear for the stimulus magnitudes employed here. Consequently, the propagation of evoked skin oscillations may be mathematically described by a wave equation of the form $L\,u(\mathbf{x},t) = 0$, where L is a linear partial differential operator encoding wave transport, $\mathbf{x}$ is a skin location, t is time, and $u(\mathbf{x},t)$ is the evoked skin

oscillation pattern. From linear systems theory, an arbitrary force stimulus $F(t)$ applied to the skin at location $\mathbf{x}_0$ evokes oscillations $u(\mathbf{x}, t)$ given by

$$u(\mathbf{x}, t) = g_{\mathbf{x}_0}(\mathbf{x}, t) * F(t), \tag{1}$$

where $*$ denotes convolution in time and $g_{\mathbf{x}_0}(\mathbf{x}, t)$ is the empirical Green's function encoding the excitation of skin oscillations evoked by an idealized unit impulse force applied at $\mathbf{x}_0$ on the respective hand. We determined the empirical Green's functions for each hand and contact location $\mathbf{x}_0$ using the impulse-driven skin oscillation measurements described above. The skin oscillations evoked by arbitrary stimuli $F(t)$ were numerically computed using Equation 1. To confirm the accuracy of this method, we compared the numerically computed oscillations with measured oscillations evoked by sinusoidal stimuli $F(t)$ with frequencies ranging from 20 to $640\,\mathrm{Hz}$. The measurement procedure was identical to the one described above, apart from the waveform. Consistent with linear systems theory, we found that the numerically computed oscillations closely approximated the actual measurements at all frequencies (Extended Data Figure 1). Because the numerical methodology avoids the need for time-intensive experiments, we used it to determine skin oscillations evoked by arbitrary stimuli in the remainder of the experiments.

Stimuli

We analyzed skin oscillations $u(\mathbf{x}, t)$ evoked by sinusoidal, diharmonic, and bandpass noise stimulus waveforms $F(t)$. For sinusoidal stimuli, $F(t) = F_0 \sin(2\pi f t)$, where f is frequency and F_0 is force amplitude. Force amplitudes were approximately $0.25\,\mathrm{N}$, except as noted. For diharmonic stimuli, $F(t) = F_1 \sin(2\pi f_1 t) + F_2 \sin(2\pi f_2 t)$, with independent force amplitudes F_1 and F_2. F_1 and F_2 were selected to ensure that the maximum evoked peak-to-peak skin displacements D_{pp} were equal, where

$$D_{pp} = \max_{\mathbf{x}} \left\{ \max_t \{u(\mathbf{x}, t)\} - \min_t \{u(\mathbf{x}, t)\} \right\}. \tag{2}$$

Bandpass noise stimuli were synthesized using a spectral Gaussian white noise algorithm[51], then bandpass filtered to the desired frequency range. Each bandpass noise stimulus was generated from the same Gaussian

white noise trace, scaled by a force amplitude F_0.

Whole-hand neural simulations

PC population spiking responses were obtained *in silico* by using the skin oscillations to drive an ensemble of spiking neuron models extracted from a simulation package (Touchsim[31], Python), similar to the methodology applied in prior work investigating PC population responses during whole-hand touch events[9]. The PC neuron models consisted of four PC types, each trained and validated in a prior study on electrophysiology recordings from non-human primates[33]. Each PC neuron model type varies slightly in its response properties (Extended Data Fig. 5a). The PC neuron models supply a nonlinear mapping from skin displacement to spiking output and accurately reproduce experimentally identified response characteristics of PCs, including response thresholds that vary across several orders of magnitude over the vibrotactile frequency range[11,13] and frequency-dependent thresholds of entrainment[10,12,14]. The stimulus amplitudes used in this work fell within the range over which the PC models were validated.

Whole-hand PC populations were assembled by sampling a random distribution weighted by spatial densities σ reported in prior studies[32,41]: $\sigma = 25/\mathrm{cm}^2$ in the distal phalanges and $\sigma = 10/\mathrm{cm}^2$ in the rest of the hand. Except where otherwise noted, the PC neuron model type for each PC in a population was randomly selected to be one of the four PC neuron model types noted above. Each PC was driven by the time-varying skin oscillations $u(\mathbf{x}_m, t)$, where $\mathbf{x}_m$ is the PC location. This produced a spike train represented as an ordered sequence $Y_m = \{t_1, t_2, ..., t_Q\}$, where t_i are spike times and Q is the number of stimulus-evoked spikes (Extended Data Fig. 2a).

PC entrainment threshold curves

Entrainment threshold curves were constructed to characterize PC frequency sensitivity. At each frequency (20 to $800\,\mathrm{Hz}$), the force amplitude of the sinusoidal input stimulus was varied to determine the entrainment threshold for each PC in the whole-hand population. The entrainment threshold was identified

as the minimum input force amplitude at which one spike was elicited per cycle of the sinusoidal stimulus. For each mth PC and frequency f, the threshold curve $E_m(f)$ recorded the maximum peak-to-peak displacement of skin oscillations evoked across the hand (D_{pp}, Equation 2) at the identified entrainment force amplitude. The maximum D_{pp} across all conditions was $100\,\mu\mathrm{m}$. In prior literature, threshold curves were determined by placing the stimulating probe near the hotspot of the terminating neuron[10–14] (Extended Data Fig. 5a). Here, however, we analyzed threshold curves for all PCs across the hand with the stimulus contact location held constant. This preserved the effects of biomechanical transmission and filtering that were not captured in prior approaches. For each PC, the preferred (most sensitive) frequency was computed as $f^* = \arg\min_f\{E_m(f)\}$. The width of each threshold curve was determined as the full width of the threshold curve (not necessarily contiguous) at half-minimum and characterized the sensitivity bandwidth of the respective PC.

Correlation analysis

The pairwise similarity of entrainment threshold curves for different PCs was assessed using the Pearson correlation coefficient c_{ij}, where i and j index the threshold curves of PCs in a population. We conducted this analysis by separating whole-hand PC populations into PC subpopulations P_k located within different distance ranges from the stimulus contact location, where $k = 0, 1, \ldots, K$ indexes the distance range. P_0 contained all N_0 PCs located within $10\,\mathrm{mm}$ of the contact location. For $k > 0$, P_k contained all N_k PCs located at distances d_k from the contact location satisfying $(20(k-1)+10) \leq d_k < (20k+10)\ \mathrm{mm}$. Distances on the 2D hand surface were computed from the SLDV geometry data using Djikstra's algorithm. We computed the mean pairwise correlation σ_k between all PC threshold curves in P_0 and all PC threshold curves in P_k as

$$\sigma_k = \frac{1}{N_0 N_k} \sum_{i=1}^{N_0} \sum_{j=1}^{N_k} c_{ij}. \tag{3}$$

We computed the mean pairwise correlation σ_0 between PC threshold curves in P_0 as

$$\sigma_0 = \frac{2}{N_0(N_0-1)} \sum_{i=1}^{N_0} \sum_{j=i+1}^{N_0} c_{ij}. \tag{4}$$

PC population spiking activity analysis

Efficient encoding hypotheses posit that neural sensory circuitry should minimize redundancy[44,52]. We assessed encoding efficiency by analyzing mean firing rates and spike timing, both of which are salient to tactile encoding[53–55]. To this end, we assembled a diverse set of stimuli encompassing commonly occurring tactile signals based on prior studies[33,34]. The stimulus set contained 60 sinusoidal, 117 diharmonic, and 50 bandpass noise stimuli that varied in amplitude and frequency parameters (see Supplementary Methods, Supplementary Table 1). We obtained spike trains evoked in whole-hand PC populations for each stimulus ($n = 227$), contact location ($n = 4$), and participant ($n = 4$ or $n = 7$ depending on the contact location).

To assess the redundancy in spiking responses of remotely located PCs, we constructed PC subpopulations P^r located within increasing distances $d_r = 20r\,\mathrm{mm}$ from the contact location. The subpopulations formed a nested array of sets, $P^1 \subset P^2 \subset \cdots \subset P^R$, successively encompassing larger numbers of PCs, N^r, where $N^r = N^{r-1} + \Delta N^r$. We analyzed spiking responses from each subpopulation using principal component analysis (PCA), interspike interval (ISI) information entropy, and spike train correlations.

Firing rate latent dimensionality analysis

To assess the latent dimensionality of spiking activity from each subpopulation r, principal component analysis (PCA) was performed on the matrix of time-averaged firing rates M^r_{mn}, where m indexed PCs and n indexed the stimuli. The data matrix M^r_{mn} was standardized across stimuli (zero-mean and unit standard deviation). To assess the latent dimensionality of the subpopulation firing rates, we computed the minimum number $B(r)$ of principal components that captured at least $99\,\%$ of the variance. A higher value of $B(r)$ indicated greater firing rate heterogeneity in subpopulation r.

Interspike interval information entropy analysis

We computed interspike intervals (ISIs) from spike trains $\mathbf{s}_m^n$ evoked in each PC m by each stimulus n. From these data, we computed normalized ISI histograms for each PC subpopulation P^r. In the main results (Fig. 4b), the histogram bin size was $\Delta t = 1\,\mathrm{ms}$ because PCs encode touch information with millisecond precision[34]. We obtained similar results for values of Δt between 0.5 and $2.0\,\mathrm{ms}$ (Extended Data Fig. 10a-g). Let p_q^r be the probability of an ISI t from P^r falling in the range $t_q \leq t < t_{q+1}$, where $t_q = q\,\Delta t$. We assessed information in spike timing by computing the Shannon information (entropy) $H(r)$, given by

$$H(r) = -\sum_{q=1}^{Q} p_q^r \log_2(p_q^r). \tag{5}$$

We also applied the same analysis to individual stimuli (Fig. 4d, Extended Data Fig. 9). Higher ISI entropy values $H(r)$ indicated more information and less redundancy in spike timing activity.

Spike train correlation analysis

We computed spike train correlations[56–58] using binned spike train vectors with bin width $\Delta t = 1\,\mathrm{ms}$ (elephant[59], Python) (Fig. 4c). We obtained similar results for values of Δt between 0.5 and $2.0\,\mathrm{ms}$ (Extended Data Fig. 10h-n). For each stimulus n and PC subpopulation P^r, we assessed pairwise spike train correlations by computing Pearson correlation coefficients $c_{ij}^n(r)$ between each pair of binned spike trains $\mathbf{s}_i^n$ and $\mathbf{s}_j^n$, where i and j index PCs in P^r. We computed the mean spike train correlation $c(r)$ for each subpopulation P^r using

$$c(r) = \frac{2}{M(M-1)N} \sum_{n=1}^{N} \sum_{i=1}^{M} \sum_{j=i+1}^{M} |c_{ij}^n(r)|, \tag{6}$$

where M is the number of PCs in a subpopulation P^r and N is the number of stimuli. Lower spike train correlations indicated less redundancy within population spike timing activity. In contrast to the ISI entropy analysis, spike train correlations took into account the relative differences in spike times between different PCs.

Data availability

The data that support the findings of this study are available from the corresponding author upon reasonable request.

References

51. Timmer, J. & König, M. On Generating Power Law Noise. *Astronomy and Astrophysics* **300,** 707–710 (1995).

52. Atick, J. J. Could information theory provide an ecological theory of sensory processing? *Network: Computation in Neural Systems* **22,** 4–44 (2011).

53. Harvey, M. A., Saal, H. P., Dammann III, J. F. & Bensmaia, S. J. Multiplexing Stimulus Information through Rate and Temporal Codes in Primate Somatosensory Cortex. *PLOS Biology* **11,** e1001558 (2013).

54. Saal, H. P., Harvey, M. A. & Bensmaia, S. J. Rate and timing of cortical responses driven by separate sensory channels. *eLife* (2015).

55. Long, K. H., Lieber, J. D. & Bensmaia, S. J. Texture is encoded in precise temporal spiking patterns in primate somatosensory cortex. *Nature Communications* **13,** 1311 (2022).

56. Bair, W., Zohary, E. & Newsome, W. T. Correlated Firing in Macaque Visual Area MT: Time Scales and Relationship to Behavior. *Journal of Neuroscience* **21,** 1676–1697 (2001).

57. Kohn, A. & Smith, M. A. Stimulus Dependence of Neuronal Correlation in Primary Visual Cortex of the Macaque. *Journal of Neuroscience* **25,** 3661–3673 (2005).

58. Cohen, M. R. & Kohn, A. Measuring and interpreting neuronal correlations. *Nature Neuroscience* **14** (2011).

59. Denker, M., Yegenoglu, A. & Grün, S. *Collaborative HPC-enabled workflows on the HBP Collaboratory using the Elephant framework* in *Neuroinformatics 2018* (2018), P19.

Acknowledgements

We thank Benoit Delhaye for feedback. We thank Polytec Inc. for the use of a vibrometry system. This research was supported by a Link Foundation Modeling, Simulation, and Training Fellowship (NT), a UCSB Graduate Opportunity Fellowship (NT), Leverhulme Trust research project grant RPG-2022-031 (HPS), and National Science Foundation award 1751348 (YV).

Author contributions

NT, GR, HPS, and YV designed the research. BD, YS, and YV collected the vibrometry data. NT, GR, and BD performed data analysis. NT, GR, HPS, and YV wrote the manuscript. All authors reviewed and edited the manuscript.

Competing interests

The authors declare no competing interests.

Additional information

Correspondence and requests for materials should be addressed to Yon Visell (yonvisell@ucsb.edu).